2013 IEEE International Conference on Robotics and Automation (ICRA)
Karlsruhe, Germany, May 6-10, 2013

Animal-inspired Design and Aerodynamic Stabilization of a Hexapedal Millirobot

Duncan W. Haldane, Kevin C. Peterson, Fernando L. Garcia Bermudez, and Ronald S. Fearing

***Abstract*— The VelociRoACH is a 10 cm long, 30 gram hexapedal millirobot capable of running at 2.7 m/s, making it the fastest legged robot built to date, relative to scale. We present the design by dynamic similarity technique and the locomotion adaptations which have allowed for this highly dynamic performance. In addition, we demonstrate that rotational dynamics become critical for stability as the scale of a robotic system is reduced. We present a new method of experimental dynamic tuning for legged millirobots, aimed at finding stable limit cycles with minimal rotational energy. By implementing an aerodynamic rotational damper, we further reduced the rotational energy in the system, and demonstrated that stable limit cycles with lower rotational energy are more robust to disturbances. This method increased the stability of the system without detracting from forward speed.**

I. Introduction

Animals have evolved an extensive variety of robust locomotion adaptations which allow for agile locomotion over diverse substrates. A number of these gaits have demonstrated remarkable open-loop stability over challenging terrain [16][25], a highly desirable attribute for legged robots operating in an unstructured environment. Using a technique called dynamic similarity scaling [1], the dynamic characteristics of a model animal can be non-dimensionalized and scaled to a size which is convenient to implement on a robotic system [7][11]. Given that dynamic scaling is an appropriate tool for designing bio-inspired robots, it remains for us to choose a suitable model animal. The Krogh principle states that "For a large number of problems there will be some animal of choice, on which it can be most conveniently studied" [18]. The American cockroach, *Periplaneta americana*, is a highly dynamic running insect, exhibiting a variety of robust and high speed gaits that we use as a model of study for the design of VelociRoACH. *P. americana* is capable of running at over 50 body-lengths per second (bl/s) and is capable of hexapedal, quadrupedal, and even bipedal locomotion [9], as well as high-speed climbing and rapid inversion [19].

Dynamic similarity scaling establishes the fundamental dynamics of a legged robotic system, but bio-mimicry is not a sufficient condition for a high-performance mobile robot.

This material is based upon work supported by the National Science Foundation under IGERT Grant No. DGE-0903711, and Grant No. CNS-0931463, and the United States Army Research Laboratory under the Micro Autonomous Science and Technology Collaborative Technology Alliance.

D.W. Haldane is with the Department of Mechanical Engineering, University of California, Berkeley, CA 94720 USA dhaldane@berkeley.edu

K.C. Peterson, F.L. Garcia Bermudez, and R.S. Fearing are with the Department of Electrical Engineering and Computer Sciences, University of California, Berkeley, CA 94720 USA {*kevincp, fgb, ronf*}*@eecs.berkeley.edu*

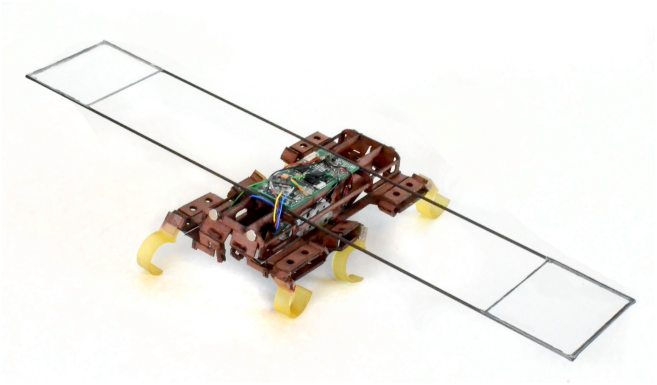

Fig. 1: The VelociRoACH: a highly dynamic bio-inspired millirobot, shown equipped with an aerodynamic stabilizer.

The dynamic tuning and optimization of iSprawl [6][17] and the RHex family of robots [23][26][10] has shown that the locomotion performance of a bio-inspired legged robot can be significantly improved. Millirobots offer significant advantages over larger scale systems [13][3], but dynamic optimization at this scale has not been sufficiently addressed. Several factors, such as limited control authority, and the necessity for minimal actuation cause dynamic tuning at the millirobotic scale to be a challenging prospect. However, there are several advantages of scale which can be exploited. Smaller systems can be more robust [15] and aerodynamic effects, which would be geometrically cumbersome at larger scales, can be readily exploited to increase locomotion performance. Prior results have shown that the addition of wings to a running robot can decrease the probability of catastrophic destabilization [20], as well as damp undesirable disturbance impulse forces [21]. In this study, we discuss the increased significance of the rotational dynamics of a robot at the small scale, and present a detailed treatment of a novel dynamic tuning methodology using aerodynamic rotational stabilization.

II. Robot Design

The main goal of this work was to create a minimally actuated, highly dynamic robotic platform which is easily steerable. VelociRoACH uses two motors, one for each side of the robot, allowing for differential steering as previously used in OctoRoACH [22]. Minimal actuation at small scales can be achieved using the Smart Composite Microstructures (SCM) process [14], which allows for the creation of lightweight linkages using planar manufacturing methods. These linkages can couple motor power input to multiple

legs, reducing the number of required actuators. Proper application of the SCM process results in highly robust, light, inexpensive, and scalable robots.

A. Dynamic Similarity

The dynamics underlying the VelociRoACH were established by the principles of dynamic similarity scaling. Dynamic scaling relies on dimensionless scaling of the parameters of a model system such that the dynamics and stability remain invariant. The dynamic scaling factors given in Table I, which were previously used to design a dynamic climbing robot from an animal template [7], are more thoroughly discussed and derived by Alexander [1]. The frequency scaling factor for the pendular climber in [7] is based on the length dependent frequency, $\omega = \sqrt{\frac{g}{L}}$, of a classical pendulum. Assuming dynamically similar systems run identically at the same non-dimensional velocity (Froude number, given by $F = \frac{v^2}{gl}$) the choice of $\alpha_\omega = \alpha_L^{-0.5}$ is also appropriate at all scales of terrestrial locomotion. This assumption is justified by animal data [1][8]. We scaled the model system to a target robot mass of 30 grams, thereby establishing the parameters found in Table I. The platform specifications found from dynamic scaling are target values, and were tuned to increase the dynamic performance of the platform, as described in the following paragraphs.

TABLE I: DYNAMIC SCALING PARAMETERS

	Scaling Factor	Value α_X	Cockroach	VelociRoACH Target	VelociRoACH Actual
Length	α_L=α_L	3.3	3.4cm	11.2cm	10cm
Mass	α_M=α_L^3	36.1	0.83g	30g	29.1g
Stiffness	α_K=α_L^2	–	–	–	40 N/m
Frequency	α_ω=$\alpha_L^{-0.5}$	0.54	27 Hz	15 Hz	24Hz
Velocity	α_V=$\alpha_L^{0.5}$	1.2	1.5 m/s	2.72 m/s	2.7 m/s
Power	α_P=$\alpha_L^{3.5}$	65.3	1.57 mW	103 mW	243 mW

P. americana's locomotion appendages are not passive monolithic structures but consist of several jointed segments which are controlled by multiple muscles. As such, the stiffness of its legs during locomotion cannot be easily measured. Thus we decided to dynamically scale the target stiffness and length of the VelociRoACH's legs down from Edubot, a 1.2 kg member of the RHex family of robots [10]. We employed 'C' shaped legs with a 2.25cm diameter which we cast from a polyurethane rubber (*Smooth On* PMC-790). The majority of the initial dynamic performance tuning focused on obtaining the correct geometry for these appendages. We used high speed video data and force plate runs to identify any dynamic aberrations in the robot's locomotion, then iterated the leg design until dynamically effective performance was achieved. The robot's legs are monolithic, therefore we cannot use kinematic adaptions to increase forward velocity as the cockroach does (see Section III). This limitation accounts for the large discrepancy in operating frequency seen in Table I.

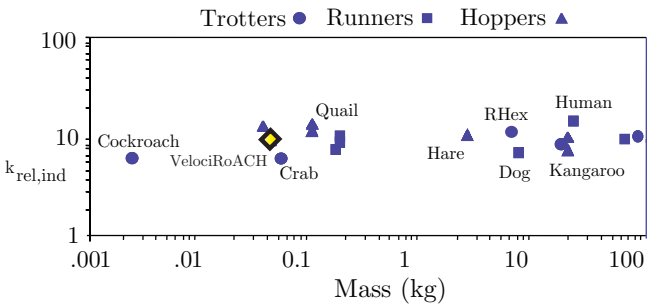

Fig. 2: Relative leg stiffness vs body mass for various animals and the VelociRoACH. Reprinted with permission from [12].

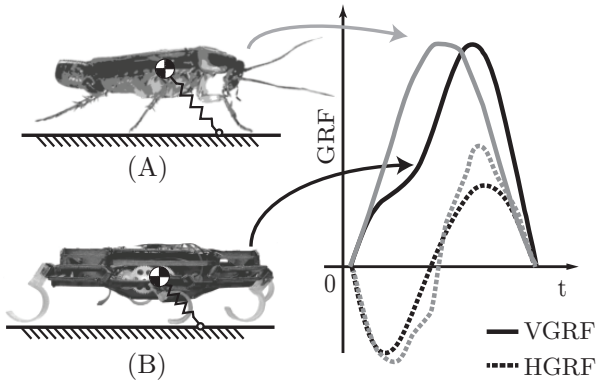

Fig. 3: Qualitative comparison of scaled and normalized horizontal and vertical ground reaction forces (HGRF, VGRF) from: (A) *P. americana* [9] and (B) the VelociRoACH.

To verify that the dynamic scaling analysis was valid, we compared the robot and animal systems via two different metrics: the relative leg stiffness, $k_{rel,ind}$, established by Blickhan and Full [4], and assessment of whole-body ground reaction forces. The calculated $k_{rel,ind}$ for the robot is 10.3, corresponding precisely with the animal data [4] (see Fig. 2). Experimentally collected ground reaction force patterns of the insect and robot are given in Fig. 3. The similarity of these ground reaction forces lends validity to the claim that the robotic and animal systems are dynamically similar. These two measures show that design by dynamic similarity has successfully preserved SLIP-like running characteristics between the animal and robotic systems. Therefore, we predict remarkable dynamic performance from the robot based on the performance of its model animal.

B. Structural Design

We implemented several design features in the robot to attain the dynamic performance of the model animal. These design adaptations are aimed at minimizing the mass of the robot, and centering it as low as possible for greater stability. The body of the VelociRoACH is comprised of a rigid structural core which houses the battery, motors, transmission, and control circuitry, and provides mechanical grounding points for the kinematic linkages. This design is a departure from previous DynaRoACH-derived robots [13][22], which placed

these components on top of the robot, significantly raising the center of gravity. In the present configuration, the motor casings provide additional stiffness to the core, reducing the amount of material required for structural integrity. The kinematic linkages attach to the core of the robot and couple rotary input from the motor to useful leg motions.

C. Kinematic Design

To design the gait kinematics for the VelociRoACH, we consider the results gleaned from the RHex family of robots. RHex uses a feed-forward clock signal known as the Buehler clock to prescribe its kinematics [24]. The Buehler clock is commonly parameterized by four variables: the touchdown and liftoff angles, (ψ_{TD}, ψ_{LO}) and the stance and flight time, (t_s, t_f). For the gait of VelociRoACH, we chose values for these variables expected to balance speed and stability. *P. americana* uses a duty factor of $\beta = \frac{t_s}{t_s+t_f} = 0.5$ [9], so we chose the stance and flight durations to be equal. The touchdown and liftoff angles were chosen to be symmetric at $(\psi_{TD}, \psi_{LO}) = \pm 42°$, as has been used previously [13]. To allow for an alternating tripod gait, the fore and aft legs are mechanically constrained $180°$ out of phase from the middle leg, as shown in Fig. 4. During straight-line running, we use a software controller (Section II-D) to enforce a $180°$ offset between the left and right sets of legs such that the contralateral middle leg of one side steps simultaneously with the fore and aft legs of the other side. With one actuator per leg, RHex has the ability to adjust its kinematics in software, allowing for highly optimized gaits [26]. The gait kinematics of VelociRoACH however, are enforced by the geometry of its kinematic linkages.

Hoover et al. determined the geometry of these linkages for the DynaRoACH robot [13], and we used a similar methodology to determine the parameters for the VelociRoACH. When the transmission was bisected down the saggital plane of the robot to allow for dual-drive actuation, we found that forces on the front and rear legs caused too much deflection in the transmission to allow for robust locomotion performance. Therefore, a planarizing parallel four-bar linkage was added to each side, as shown in Fig. 4. These linkages minimized the potential energy stored in the transmission while maximizing its stiffness to off axis loading. They also allowed the reduction of the mass of the recirculating transmission layer by 57%, the movement of which excites parasitic oscillation modes during locomotion.

D. Motor Transmission and Control Electronics

The VelociRoACH uses two 7 mm, $3.3\,\Omega$ coreless brushed DC motors (Didel # Mk07-3.3) to drive its legs, with each side of the robot driven independently. To enable locomotion across a range a frequencies ($4-24$ Hz), we selected a gear ratio of $16:1$.

A lightweight electronics package controls the robot's locomotion and logs data from its on-board sensors [2]. It includes a 40 MHz microprocessor, an inertial measurement unit, an 802.15.4 wireless radio, and motor control circuitry[1].

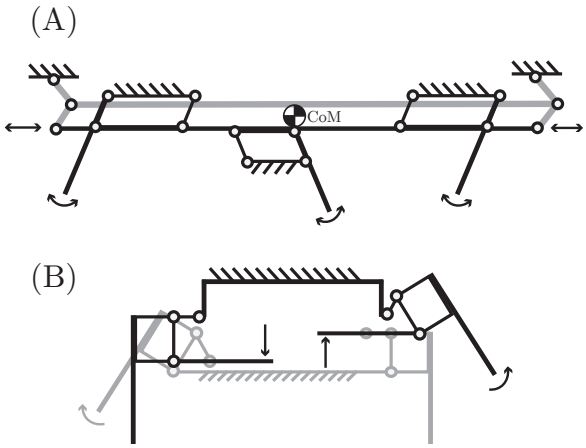

Fig. 4: Views of the kinematic linkages from the side (A) and rear (B).

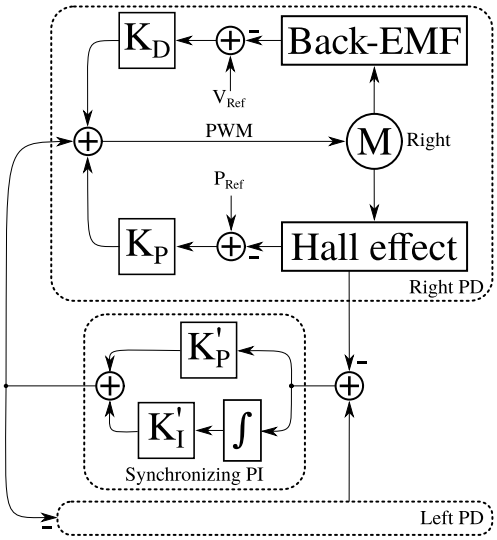

Fig. 5: Locomotion controller block diagram. The Left PD block is identical to the Right PD block.

Telemetry data is logged to an on-board flash memory at 300 Hz and later downloaded wirelessly to a computer for analysis. Each motor is equipped with magnetic incremental encoders. The encoders, along with the motor back EMF signal, feed a 1 KHz control loop[2].

The main locomotion control loop, shown in Fig. 5, consists of two independent control laws. A low gain, proportional derivative feedback controller (Right/Left PD) runs on each motor to maintain the desired leg frequency. Hall effect encoders and the back EMF signal from the motors provide the position and velocity of the motor respectively. In addition to this controller, a synchronizing proportional integral (PI) control law enforces the desired phase offset between the motors. The independent control laws provide several benefits. At the highest stride frequencies, the motor is speed limited (see Fig. 11) and the control bandwidth is

[1]Embedded board: https://github.com/biomimetics/imageproc_pcb

[2]Embedded code: https://github.com/biomimetics/octoroach

subsequently reduced. High proportional gain in the synchronizing control law ensures that maintaining the phase offset between the motors is prioritized and the desired gait is preferentially maintained. The integral term in the synchronizing control law accounts for variations between the two motors, eliminating the need to characterize each motor. The independent control laws also allow the controller's response to gait and speed variations to be independently and more intuitively tuned. The VelociRoACH can also run with the control loop disabled by simply commanding an open loop motor PWM. At certain PWM duty cycles, the gait will passively converge to alternating tripod and the robot will run stably, otherwise open loop performance is unreliable.

III. Dynamic Performance and Stabilization

P. americana adjusts its limb kinematics to increase speed while keeping its stride frequency relatively constant [9]. This adaptation allows the animal to operate in a single resonant regime, which is desirable for effective and robust locomotion across a range of speeds. Due to the minimally actuated nature of the VelociRoACH, the kinematics are invariant. Therefore, we examined the stride frequency dependent dynamic response of the robot to find a desirable operating regime.

Legged locomotion is characterized by periodic trajectories (limit cycles) of the system dynamics. As the scale of a robot is reduced, the rotational dynamics of the system have a larger effect on the motion of the robot: the moment of inertia, $I = mr^2$, scales with α_L^5. For a given, size-specific, perturbation we expect a millirobot to rotate far more than a larger robot. For example: Edubot undergoes roll oscillations of 1° during steady state locomotion [5], whereas the 30 gram VelociRoACH can experience 25° roll rotations during stable locomotion. While some amount of rotational oscillation can stabilize the system [5], limit cycles with high rotational energy–coupled with low inertia–can increase the chance of a disturbance causing catastrophic failure. We therefore focused our dynamic tuning efforts on finding highly robust, passively stable limit cycles with minimal rotational energy.

A. Roll Stabilizer

During steady state running, the VelociRoACH has significant roll oscillations, as shown in Fig. 6. These oscillations arise as a dynamic effect due to alternating tripod kinematics wherein one side of the robot has twice the effective stiffness as the other [5]. To reduce the roll oscillations, we add an aerodynamic stabilizer consisting of two rectangular sections, measuring 5cm x 4cm, of 50 μm PET oriented parallel to the direction of forward travel. These airfoils are rigidly constrained by a carbon fiber frame at a distance of 15cm from the center of the robot (see Fig. 1). As a control between the inertial and aerodynamic effects, we also examine the performance of the stabilizer with the PET airfoils removed. The aerodynamic stabilizer is specifically designed to damp roll oscillations, while being lightweight and having minimal drag in the forward direction. A significant aerodynamic

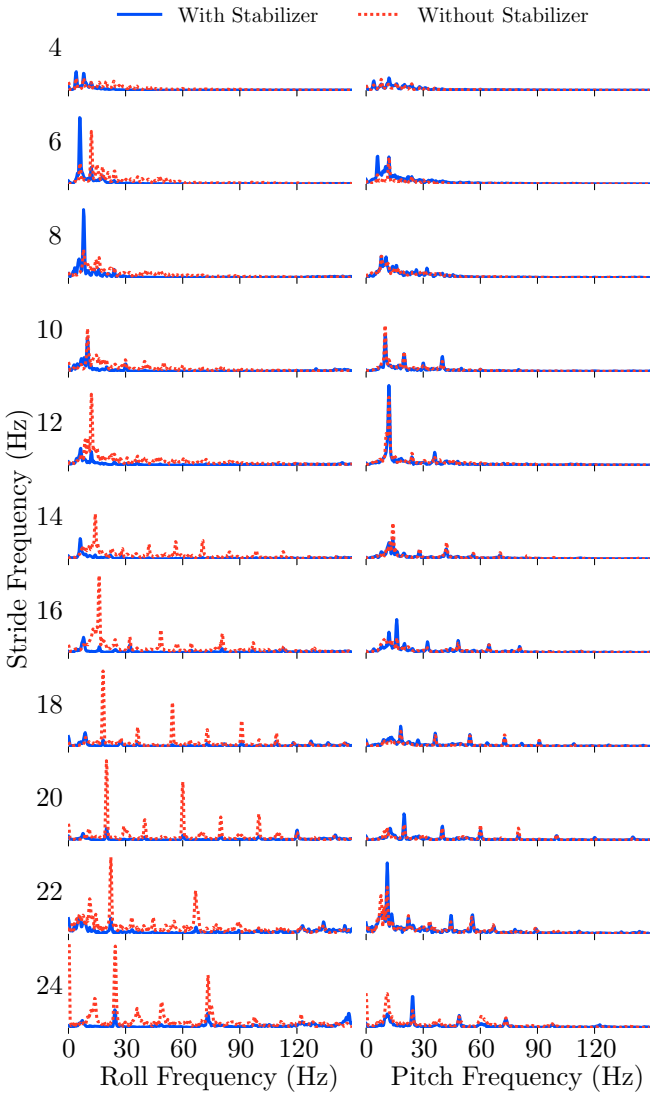

Fig. 6: Frequency spectra of the robot's oscillations with and without the aerodynamic stabilizer plotted as a function of the commanded stride frequency. Oscillatory energy in the roll axis was the highest of all the rotational components prior to the addition of the stabilizer. The stabilizer effectively filters this energy at higher stride frequencies. Yaw oscillations (not shown) are relatively unaffected by the stabilizer and have a peak magnitude of 904 $^\circ$/s.

force results when the robot rolls during high-speed running due to the high drag nature of a flat plate. We computed the differing inertias of the robot with and without the roll stabilizer using a CAD model of the robot and verified them in part using rigid body pendulum experiments. The form of the inertia tensors is given in (1), where x, y and z are the roll, pitch, and yaw axes, respectively. The standard robot has inertia, $\mathbf{I_0}$ (2); $\mathbf{I_S}$ (3) corresponds to the robot with the stabilizer.

$$\mathbf{I} = \begin{bmatrix} I_{xx} & I_{xy} & I_{xz} \\ I_{yx} & I_{yy} & I_{yz} \\ I_{zx} & I_{zy} & I_{zz} \end{bmatrix} \text{ kg mm}^2 \quad (1)$$

$$\mathbf{I_O} = \begin{bmatrix} 9.29 & -0.12 & -0.22 \\ -0.12 & 21.51 & 0.007 \\ -0.22 & 0.007 & 21.97 \end{bmatrix} \text{ kg mm}^2 \quad (2)$$

$$\mathbf{I_S} = \begin{bmatrix} 28.52 & -0.12 & -0.23 \\ -0.12 & 23.12 & 0.005 \\ -0.23 & 0.005 & 45.92 \end{bmatrix} \text{ kg mm}^2 \quad (3)$$

B. Steady State Running

Telemetry data was captured for the VelociRoACH running on closed-loop carpet at stride frequencies in the $4-25$ Hz range. In particular, tri-axial gyroscope data was logged at 300 Hz during each run (repeated three times). We discarded the leading one second of each trial to remove any transient effects. To better understand the nature of the VelociRoACH oscillations as a function of the stride frequency, we used Python[3] to compute the fast Fourier transform of each run, first passed through a Hann window, and then averaged across repeated trials. The resulting frequency spectra are plotted for pitch and roll in Fig. 6. Roll shows a large degree of oscillation without the stabilizer, visible throughout the spectra and reaching up to the fifth harmonic of the commanded stride frequency. This motivated the addition of the stabilizer on the roll axis, and Fig. 6 shows this approach was successful at reducing the degree of roll oscillations. Both pitch and yaw, which have less oscillations to begin with, are relatively unaffected by the added stabilizer.

We analyzed the gyroscope data to determine the amount of rotational energy the robot possesses in each stable limit cycle. To find the energy, we first parameterize the data by the accumulated stride phase, ϕ, which is the total angular rotation of the output link from the beginning of the trial. The rotational energy is calculated using the angular velocities measured from the on board gyroscope with

$$E_{Rot}(\phi) = \frac{1}{2}\omega(\phi)^T I \omega(\phi). \quad (4)$$

The energy is then divided into individual strides

$$E^n_{Rot}(\phi) = E_{Rot}(\phi) : 2\pi(n-1) \leq \phi < 2\pi n, \quad (5)$$

where n represents the stride number. The average and variance among $k = 10$ successive strides is then computed from

$$\bar{E}_{Rot}(\phi) = \frac{1}{k}\sum_{n=1}^{k} \bar{E}^n_{Rot}(\phi) \quad (6)$$

and

$$\sigma(E_{Rot}(\phi))^2 = \frac{1}{k-1}\sum_{n=1}^{k} (E^n_{Rot}(\phi) - \bar{E}_{Rot}(\phi))^2. \quad (7)$$

As a metric of performance, we define the mean rotational energy during a stride to be

$$\bar{E}_{Rot} = \frac{1}{2\pi}\int_0^{2\pi} \bar{E}_{Rot}(\phi)\, \mathrm{d}\phi. \quad (8)$$

[3]Scientific Tools for Python: http://www.scipy.org/

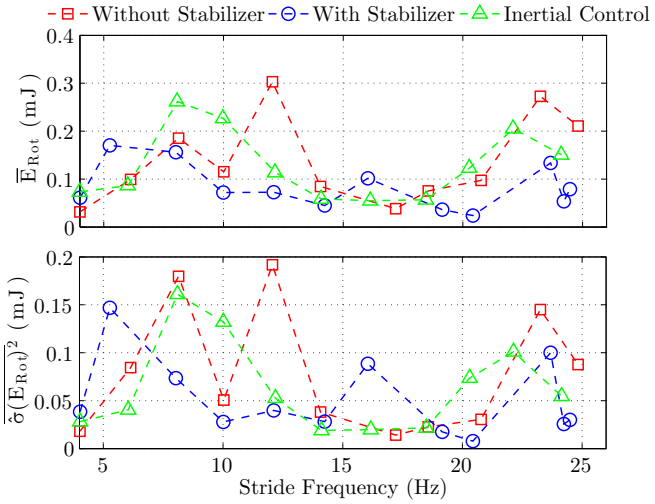

Fig. 7: Lowest energy limit cycle for each treatment [Top] and average variation in the rotational energy over the course of a stride [Bottom].

An additional metric, the mean normalized variance in energy over a stride is given by

$$\overline{\hat{\sigma}(E_{Rot})^2} = \frac{1}{2\pi}\int_0^{2\pi} [\sigma(E_{Rot}(\phi))^2 / \bar{E}_{Rot}(\phi)]\, \mathrm{d}\phi. \quad (9)$$

Fig. 7 shows the effect of both the aerodynamic stabilizer and the inertial control configuration on the system. At low frequencies, the higher inertias of the aerodynamic stabilizer and the inertial control increase the total energy. A local minimum in average frequency is found for the unmodified and inertial control case at 16 Hz, near the dynamically scaled frequency of the robot (see Table I). By contrast, with the aerodynamic stabilizer equipped, the range of frequencies with low energy limit cycles is increased, reducing the robot's reliance on a single well-tuned frequency. We observe a clear decrease in the average energy over all frequencies ≥ 10 Hz for the aerodynamically stabilized robot when compared to the unmodified and inertial control cases. We also consider the robot's ability to passively maintain stable limit cycles while running in the presence of small perturbations, such as foot slip and ground contact variations. The variation in energy between successive strides shown in Fig. 7 provides a measure of the periodicity of locomotion and of how robust the limit cycle is to small disturbances. Both the aerodynamic stabilizer and the inertial control show less variation in response to small perturbations. By contrast, the unmodified robot shows generally higher variation, and significantly higher variation at some frequencies. The lower inertia of the unmodified robot increases its susceptibility to small disturbances and correspondingly decreases the stability margin of the robot.

C. Disturbance Rejection

In addition to increasing robustness to small perturbations, we hypothesized that the aerodynamic damper would allow the robot to recover more quickly from large perturbations.

TABLE II: AVERAGE DISTURBANCE RESPONSE

Stride frequency		Configuration	
		Without Stabilizer	With Stabilizer
16 Hz	Ts	0.37 s	0.18 s
	$\bar{E}_{\text{Disturb}}$	1.15 mJ	0.37 mJ
	S_{Disturb}	435 $\mu J \cdot s$	66 $\mu J \cdot s$
20 Hz	Ts	0.29 s	0.24 s
	$\bar{E}_{\text{Disturb}}$	1.97 mJ	0.74 mJ
	S_{Disturb}	578 $\mu J \cdot s$	186 $\mu J \cdot s$

To assess the validity of this hypothesis, we ran the robot over a known obstacle, in this case a vertical step equal to 35% of its hip height. We measured the departure of body-centric metrics away from the median state and their subsequent recovery. The robot is more prone to locomotion failures due to excessive body rotation so we chose the body-centric parameter to be the rotational energy in the system. This was chosen over any individual component of rotation because the specific response of the robot is highly sensitive to when in the stride the disturbance was encountered, the robot's stride frequency, and whether or not the aerodynamic stabilizer was equipped. Therefore, the rotational energy of the system is a more robust indicator of the perturbed state of the robot. To account for the variations in the rotational energy due to the periodic motion of the robot, a moving average filter was applied with a window size equal to the length of a single stride. We selected the settling time of the robot, T_s, as a disturbance rejection metric. The settling time is defined as the time that 80% of the maximum energy increase due to the disturbance takes to dissipate. We also calculated the average increase in rotational energy from the perturbation,

$$\bar{E}_{\text{Disturb}} = \frac{1}{T_s} \int_{t_0}^{t_0+T_s} (E(t) - \bar{E}_{\text{steadystate}})\, \mathrm{d}t, \qquad (10)$$

and the action of the disturbance,

$$S_{\text{Disturb}} = T_s \cdot \bar{E}_{Disturb} \qquad (11)$$

as additional figures of merit.

Representative step responses of the robot running at 16 Hz with and without the stabilizer are shown in Fig. 8a and 8b. The robot encounters the step at time t_0 and the transient response duration is shaded in gray. Table II summarizes the results of the disturbance rejection experiments (N≥3). The robot equipped with stabilizer shows increased performance across all metrics at both stride frequencies tested. Along with rejecting the disturbance more quickly, the aerodynamic stabilizer also reduced the amount of energy injected into the system by the disturbance. The action of the disturbance is reduced by a factor of six at 16 Hz and a factor of three at 20 Hz, demonstrating the success of the aerodynamically stabilized robot at initially rejecting and quickly recovering from the disturbance.

IV. RESULTS

Fig. 9 shows the speed of the robot as a function of commanded stride frequency. The aerodynamic stabilizer

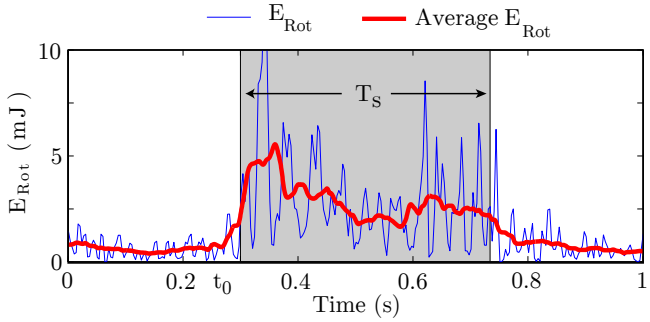

(a) Without Stabilizer

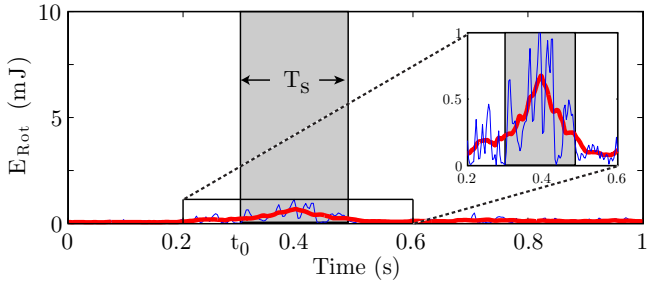

(b) With Stabilizer

Fig. 8: Representative energetic disturbance and stabilization response to a step perturbation while running at 16 Hz. The average energy is computed using a moving average filter with a window size equivalent to the length of a single stride. T_s represents the duration of the transient response, which is shaded in gray.

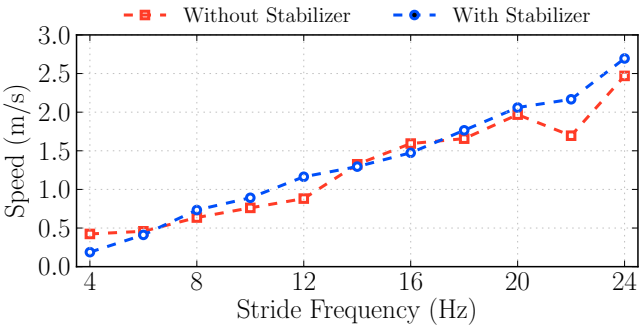

Fig. 9: Robot speed with and without roll stabilizers as a function of the commanded stride frequency.

improved the robot's reliability at the higher speeds, with zero incidents of catastrophic destabilization, which were occasionally observed in the unmodified configuration. There is no measurable effect from the stabilizers on the forward progress of the robot. The addition of the roll stabilizer did not slow the robot, as might have been expected from additional aerodynamic drag.

In addition to measuring the speed of the VelociRoACH, we calculated the specific resistance, $SR = \frac{P}{mgv}$ (see Fig. 10), which is the power required per Newton of robot per m/s of velocity. As stride frequency increases, we see an initial negative trend followed by a nearly constant region and then

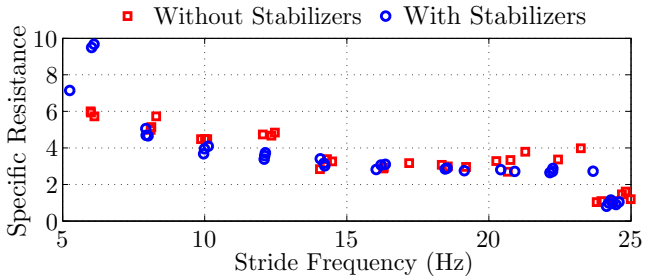

Fig. 10: Specific Resistance as a function of stride frequency.

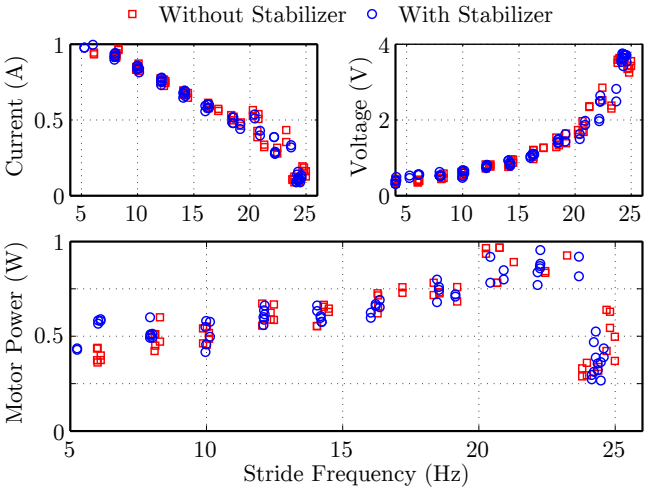

Fig. 11: Individual motor performance as a function of stride frequency. These curves are representative of a lightly loaded, speed-limited motor.

a sharp reduction as the motor reaches the terminus of its speed limited regime.

Fig. 11 shows the voltage, current, and power of the motors across the frequencies of operation. Due to the efficient flexure-based transmission and energy storage and return from the compliant legs, very little torque (and thus current) is needed to drive the legs at the highest frequencies. From work-loop experiments performed using a muscle lever, we found that only 15 μJ were dissipated per leg compression. This leads to highly efficient high-speed running, as seen from the drop in motor power at high speeds. These motor dynamics lead to the unintuitive result that the robot uses the least amount of power when operating at its maximum speed. A sufficient condition for this scenario is that the motor be as minimally loaded as possible, which is achievable at the millirobotic scale with proper mechanical design and well tuned dynamics.

In addition to straight-line running on level surfaces, we performed several experiments that assessed the capabilities of the robot when operating in unstructured environments where legged locomotion is preferable over wheels. As shown in Fig. 12, the VelociRoACH is capable of rapidly traversing obstacles over 3.2 cm in height (greater than the hip height of the robot). The robot also locomotes effectively over rough terrain, and can scale slopes equal to the critical

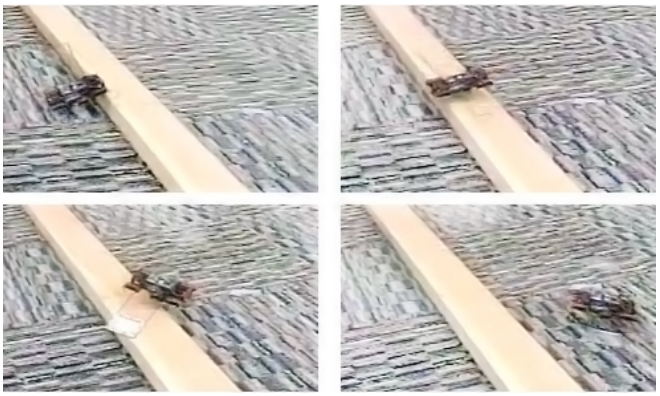

Fig. 12: Stills from the accompanying video showing the robot traversing a large obstacle

angle of repose for small ($\sim$1 cm diameter) gravel. This indicates that the robot can operate in any physical terrain made of this, or similar, substrate. The maximum measured payload capacity for the VelociRoACH is 125 grams, over four times the nominal body mass. Due to the low power consumption at the maximum operating frequency, the robot has a projected battery life of 27 minutes at its maximum speed, and a theoretical range of 4.43 km over level ground.

V. Conclusions and Future Work

Using dynamic scaling principles and design adaptations for high speed running, we successfully designed and fabricated a highly dynamic hexapedal millirobot, capable of autonomous operation in an unstructured environment. The VelociRoACH is capable of running at 27 body-lengths per second (2.7 m/s) making it, relative to scale, the fastest untethered legged robot built to date. By minimizing the load required to sustain locomotion, we were able to achieve minimal power consumption at the highest operating frequency by operating our motors in a speed-limited regime. This design adaptation allowed the VelociRoACH to achieve a specific resistance of 0.98 while running at 2.7 m/s, indicating uncommon dynamic performance for a robot of this scale, as shown in Table III.

By simple inspection of relative scales, we found that a robot's rotational dynamics become critical for stability as the size scale of a robot is reduced. We developed a new gait tuning methodology for millirobots which aims at finding stable limit cycles which minimize the amount of rotational energy in the system. We experimentally searched for these limit cycles across the broad stride frequency spectrum ($4 - 25$ Hz) achievable by the robot, and found favorable regions for operation. The novel addition of an aerodynamic roll damper reduced the rotational energy for all stable limit cycles which corresponded to a forward speed of over 1.0 m/s, and expanded the range of frequencies at which low energy limit cycles were found. We compared the relative stability margins using the settling time as a metric for the robot with and without the stabilizer. We found that for a given disturbance, limit cycles with reduced rotational energy were perturbed less from their mean state

TABLE III: COMPARISON TO SIMILAR ROBOTS

	VelociRoACH	**DynaRoACH** [13]	**DASH** [3]	**iSprawl** [17]	**Research RHex** [26]
External Dimensions (LxWxH) (cm)	10 x 6.5 x 4.2	10 x 4.5 x 3	10 x 5 x 10	15.5 x 11.6 x 0.7	54 x 39 x 12
Mass (g)	29.1	23.7	16.2	300	8200
Top Speed (body-lengths/second)–(m/s)	27 (2.7)	14 (1.4)	15 (1.5)	15 (2.3)	5 (2.7)
Stride Frequency (Hz)	24	20	17	14	6
Specific Resistance	0.98	1.1	1.42	1.75	0.72

and recovered more quickly. These results demonstrate the validity of our new dynamic tuning approach for millirobotic locomotion. We therefore conclude that aerodynamic locomotion adaptations can aid small scale robots operating in unstructured environments.

Although the VelociRoACH is fully capable of effective locomotion at high speeds, we found that the addition of an aerodynamic stabilizer increased its capacity to reject environmental disturbances. Future work should accurately model the aerodynamic effect the dampers produce, and use that information to optimize their geometry for both forward velocity and stability. The large size of the stabilizer adversely effects the robot's mobility in cluttered environments, so it would be valuable to explore other potentially collapsible wing configurations. An in-depth statistical analysis on an extensive set of data will be used to formally determine the effect of the stabilizer on the variability of the robot's performance.

ACKNOWLEDGMENTS

The authors would like to thank the Center for Integrative Biomechanics in Education and Research for allowing the use of their force platform and muscle lever to perform experiments. Thanks also to the members of the Biomimetic Millisystems Lab for their helpful comments and discussions.

REFERENCES

[1] R. M. Alexander, *Principles of Animal Locomotion*. Princeton University Press, 2003.

[2] S. S. Baek, F. L. Garcia Bermudez, and R. S. Fearing, "Flight control for target seeking by 13 gram ornithopter," *2011 IEEE/RSJ Int. Conf. on Intelligent Robots and Systems*, pp. 2674–2681, Sept. 2011.

[3] P. Birkmeyer, K. Peterson, and R. S. Fearing, "DASH : A dynamic 16g hexapedal robot," *Int.Conf. on Intelligent Robots and Systems*, pp. 2683–2689, 2009.

[4] R. Blickhan and R. J. Full, "Similarity in multilegged locomotion: Bouncing like a monopode," *Jnl. of Comparative Physiology A: Neuroethology, Sensory, Neural, and Behavioral Physiology*, vol. 173, no. 5, pp. 509–517, 1993.

[5] S. Burden, J. E. Clark, J. D. Weingarten, H. Komsuoglu, and D. E. Koditschek, "Heterogeneous Leg Stiffness and Roll in Dynamic Running," *IEEE Int.Conf. on Robotics and Automation*, pp. 4645–4652, Apr. 2007.

[6] J. E. Clark and M. R. Cutkosky, "Stability measure comparison for the design of a dynamic running robot," *Climbing and Walking Robots*, vol. 4, pp. 261–268, 2006.

[7] J. E. Clark, D. I. Goldman, P.-c. Lin, G. a. Lynch, T. S. Chen, H. Komsuoglu, R. J. Full, and D. E. Koditschek, "Design of a bio-inspired dynamical vertical climbing robot," *Robotics: Science and Systems*, 2007.

[8] C. T. Farley, J. Glasheen, and T. A. McMahon, "Running springs: speed and animal size." *Jnl. of Experimental Biology*, vol. 185, pp. 71–86, Dec. 1993.

[9] R. J. Full and M. S. Tu, "Mechanics of a rapid running insect: two-, four- and six-legged locomotion." *Jnl. of Experimental Biology*, vol. 156, pp. 215–31, Mar. 1991.

[10] K. C. Galloway, J. E. Clark, M. Yim, and D. E. Koditschek, "Experimental Investigations into the Role of Passive Variable Compliant Legs for Dynamic Robotic Locomotion," in *IEEE Int. Conf. on Robotics and Automation*, 2011, pp. 1243–1249.

[11] D. I. Goldman, T. S. Chen, D. M. Dudek, and R. J. Full, "Dynamics of rapid vertical climbing in cockroaches reveals a template." *The Journal of Experimental Biology*, vol. 209, pp. 2990–3000, Aug. 2006.

[12] P. Holmes, R. J. Full, D. Koditschek, and J. Guckenheimer, "The Dynamics of Legged Locomotion: Models, Analyses, and Challenges," *SIAM Review*, vol. 48, no. 2, pp. 207–304, Jan. 2006.

[13] A. M. Hoover, S. Burden, X. Y. Fu, S. S. Sastry, and R. S. Fearing, "Bio-inspired design and dynamic maneuverability of a minimally actuated six-legged robot," in *3rd IEEE RAS and EMBS Int. Conf. on Biomedical Robotics and Biomechatronics (BioRob)*, Sept. 2010, pp. 869–876.

[14] A. M. Hoover and R. S. Fearing, "Fast scale prototyping for folded millirobots," *IEEE Int. Conf. on Robotics and Automation*, pp. 886–892, 2008.

[15] K. Jayaram, J. M. Mongeau, B. McRae, and R. J. Full, "High-speed horizontal to vertical transitions in running cockroaches reveals a principle of robustness," in *Society for Integrative and Comparative Biology*, 2010.

[16] D. L. Jindrich and R. J. Full, "Dynamic stabilization of rapid hexapedal locomotion." *Jnl. of Experimental Biology*, vol. 205, pp. 2803–23, Sept. 2002.

[17] S. Kim, J. E. Clark, and M. R. Cutkosky, "iSprawl: Design and Tuning for High-speed Autonomous Open-loop Running," *The Int. Jnl. of Robotics Research*, vol. 25, no. 9, pp. 903–912, Sept. 2006.

[18] A. Krogh, "The Progress of Physiology," *The American Journal of Physiology*, pp. pp. 243–251, 1929.

[19] J.-M. Mongeau, B. McRae, A. Jusufi, P. Birkmeyer, A. M. Hoover, R. S. Fearing, and R. J. Full, "Rapid inversion: running animals and robots swing like a pendulum under ledges." *PloS one*, vol. 7, no. 6, p. e38003, Jan. 2012.

[20] K. Peterson, P. Birkmeyer, R. Dudley, and R. S. Fearing, "A wing-assisted running robot and implications for avian flight evolution," *Bioinspiration & Biomimetics*, vol. 6, no. 4, p. 46008, 2011.

[21] K. Peterson and R. S. Fearing, "Experimental dynamics of wing assisted running for a bipedal ornithopter," in *IEEE Int. Conf. on Intelligent Robots and Systems*, 2011, pp. 5080–5086.

[22] A. Pullin, N. Kohut, D. Zarrouk, and R. S. Fearing, "Dynamic turning of 13 cm robot comparing tail and differential drive," *IEEE Int. Conf. on Robotics and Automation*, 2012.

[23] U. Saranli, M. Buehler, and D. E. Koditschek, "RHex: A Simple and Highly Mobile Hexapod Robot," *The International Journal of Robotics Research*, vol. 20, no. 7, pp. 616–631, July 2001.

[24] J. E. Seipel and P. J. Holmes, "A simple model for clock-actuated legged locomotion," *Regular and Chaotic Dynamics*, vol. 12, no. 5, pp. 502–520, Oct. 2007.

[25] S. Sponberg and R. J. Full, "Neuromechanical response of musculoskeletal structures in cockroaches during rapid running on rough terrain." *Jnl. of Experimental Biology*, vol. 211, pp. 433–46, Feb. 2008.

[26] J. D. Weingarten, G. A. D. Lopes, M. Buehler, R. E. Groff, and D. E. Koditschek, "Automated Gait Adaptation for Legged Robots," *IEEE Int. Conf. on Robotics and Automation*, 2004.